Small molecule perimeter defense in entomopathogenic bacteria

Jason M. Crawford[a,1,2], Cyril Portmann[a,1], Xu Zhang[b], Maarten B. J. Roeffaers[b,3], and Jon Clardy[a,b,4]

[a]Department of Biological Chemistry and Molecular Pharmacology, Harvard Medical School, Boston, MA 02115; and [b]Department of Chemistry and Chemical Biology, Harvard University, Cambridge, MA 02138

Edited by Jerrold Meinwald, Cornell University, Ithaca, NY, and approved May 3, 2012 (received for review January 20, 2012)

Two Gram-negative insect pathogens, *Xenorhabdus nematophila* and *Photorhabdus luminescens*, produce rhabduscin, an amidoglycosyl- and vinyl-isonitrile-functionalized tyrosine derivative. Heterologous expression of the rhabduscin pathway in *Escherichia coli*, precursor-directed biosynthesis of rhabduscin analogs, biochemical assays, and visualization using both stimulated Raman scattering and confocal fluorescence microscopy established rhabduscin's role as a potent nanomolar-level inhibitor of phenoloxidase, a key component of the insect's innate immune system, as well as rhabduscin's localization at the bacterial cell surface. Stimulated Raman scattering microscopy visualized rhabduscin at the periphery of wild-type *X. nematophila* cells and *E. coli* cells heterologously expressing the rhabduscin pathway. Precursor-directed biosynthesis created rhabduscin mimics in *X. nematophila* pathway mutants that could be accessed at the bacterial cell surface by an extracellular bioorthogonal probe, as judged by confocal fluorescence microscopy. Biochemical assays using both wild-type and mutant *X. nematophila* cells showed that rhabduscin was necessary and sufficient for potent inhibition (low nM) of phenoloxidases, the enzymes responsible for producing melanin (the hard black polymer insects generate to seal off microbial pathogens). These observations suggest a model in which rhabduscin's physical association at the bacterial cell surface provides a highly effective inhibitor concentration directly at the site of phenoloxidase contact. This class of molecules is not limited to insect pathogens, as the human pathogen *Vibrio cholerae* also encodes rhabduscin's aglycone, and bacterial cell-coated immunosuppressants could be a general strategy to combat host defenses.

oxidase inhibitors | innate immunity | natural products | virulence factors

Xenorhabdus and *Photorhabdus* species are enteric mutualistic gammaproteobacteria of their respective *Steinernema* and *Heterorhabditis* nematode hosts (1–3). The free-living infective juvenile-stage nematode hunts insect larvae in the soil, invades the insect's circulatory system, and regurgitates its mutualistic bacteria to initiate insect pathogenesis (entomopathogenesis). The bacteria produce an assortment of small molecules and proteins to regulate the multipartite symbiosis by overcoming the insect's innate immune system, killing the insect host and microbial competitors, and supporting proper nematode development. A bacteria–nematode pair can efficiently parasitize a range of insect larvae, making the duo an effective biocontrol agent in agricultural applications. The bacteria's coordination of two vastly different objectives in two different animal hosts provides an excellent model system for investigating mutualistic and pathogenic bacteria–animal interactions (1–3).

We previously found that the bacterial uptake of L-proline, an abundant amino acid in insect hemolymph, enhanced the bacterial proton motive force and antibiotic production in the primary-phase phenotypic variants of *X. nematophila* ATCC19061 and *P. luminescens* TT01 (4). Rhabduscin (structure **1**), a tyrosine-derived amidoglycosyl- and vinyl-isonitrile product (Fig. 1), was up-regulated in *X. nematophila* by about an order of magnitude in L-proline–supplemented cultures. A candidate rhabduscin gene cluster was identified in the *X. nematophila* ATCC19061 genome (5) by homology to the known isonitrile-forming biosynthetic genes *isnA* and *isnB* (6, 7) along with a glycosyltransferase, and this analysis was validated by heterologous production of rhabduscin in genetically transformed *Escherichia coli* (4). The *P. luminescens* TT01 genome (8) also contained the rhabduscin biosynthetic genes, and rhabduscin production was detected in this genus as well. A structurally related molecule, byelyankacin (structure **2**), which was first identified in an *Enterobacter* species (9) and then later in metagenomic libraries (10), exhibits potent human melanogenesis–inhibitory activity by inhibiting tyrosinase—a phenoloxidase-type enzyme. Taken together, these observations led to the proposal that rhabduscin's natural function is inhibiting the melanin-producing insect phenoloxidase (PO), a critical enzymatic innate immune response to invading pathogens (4).

Innate immunity is a largely conserved feature in animals, and the insect's immune system parallels vertebrate innate immunity in many regards (11). The insect has pattern-recognition receptors (PRRs) that, upon microbial invasion, recognize pathogen-associated molecular patterns (PAMPs) and mount both humoral and cellular immune responses with high spatial and temporal control (12). In the pro-PO system, PAMP recognition stimulates a serine protease cascade leading to pro-PO cleavage and catalytically competent PO (13, 14). PO is the terminal component in invertebrate innate immunity that accepts phenolic substrates initially to generate short-lived cytotoxic quinone products, which are in turn converted to the long-lived and rigid polymer called melanin. The tightly controlled activation of the melanization complex, which binds to bacterial cells and polysaccharides, leads to localization of cytotoxic products around and melanin deposition directly on the intruding microorganism, encapsulating the pathogen. PO also enhances pathogen phagocytosis by hemocytes and contributes in wound healing by sclerotization, providing a formidable defense against microbial invaders (13, 14).

While *P. luminescens* was previously shown to produce multipotent bacterial stilbenes that exhibit micromolar PO inhibition against the model *Manduca sexta* insect larvae and contribute to virulence (15–17), rhabduscin's natural role has not been experimentally assessed. To assign a specific function to rhabduscin in immunosuppression, we began a detailed investigation of rhabduscin's cellular localization and biological activity. Here, we

Author contributions: J.M.C., C.P., and J.C. designed research; J.M.C., C.P., X.Z., and M.B.J.R. performed research; J.M.C., C.P., X.Z., and M.B.J.R. contributed new reagents/analytic tools; J.M.C., C.P., X.Z., M.B.J.R., and J.C. analyzed data; and J.M.C., C.P., and J.C. wrote the paper.

The authors declare no conflict of interest.

This article is a PNAS Direct Submission.

Freely available online through the PNAS open access option.

[1]J.M.C. and C.P. contributed equally to this work.

[2]Present address: Department of Chemistry, Chemical Biology Institute, Yale University, New Haven, CT 06520.

[3]Present address: Department of Microbial and Molecular Systems, Katholieke Universiteit Leuven, B-3001 Heverlee, Belgium.

[4]To whom correspondence should be addressed. E-mail: jon_clardy@hms.harvard.edu.

This article contains supporting information online at www.pnas.org/lookup/suppl/doi:10.1073/pnas.1201160109/-/DCSupplemental.

BIOCHEMISTRY

CHEMISTRY

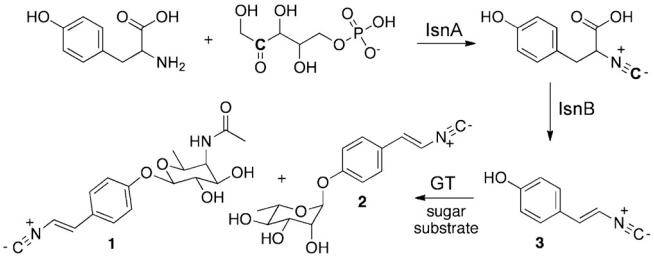

Fig. 1. Rhabduscin (**1**) and byelyankacin (**2**) biosynthesis.

demonstrate that rhabduscin harbors a potent nanomolar-level immunosuppressive activity against PO, which is dramatically more potent than the previously described stilbenes. Strikingly, rhabduscin binds at the periphery of bacterial cells, as visualized by stimulated Raman scattering and confocal fluorescence microscopic techniques, where its location and potent PO-inhibitory activity contribute substantially to virulence.

Results and Discussion

Rhabduscin Biosynthesis and its Cellular Localization. The organization of the biosynthetic genes for rhabduscin (**1**) in *P. luminescens* differs dramatically from that found in *X. nematophila*, and heterologous expression in *E. coli* was used to clarify the differences. In *X. nematophila*, we recently demonstrated that a small three-gene cluster (XNC1_1221-XNC1_1223), which includes *isnA*, *isnB*, and a glycosyltransferase gene, conferred rhabduscin production in the heterologous host *E. coli* (4). Genome synteny analysis, using the MicroScope bioinformatics platform (18), showed a similar set of genes in *P. luminescens*, but a large gap, more than 1,000 genes, separated *isnA* and *isnB* (*plu2816* and *plu2817*) from two glycosyltransferase homologs (*plu1760* and *plu1762*) (Fig. 2*A*). It seemed likely that both glycosyltransferase genes contributed to rhabduscin biosynthesis in the *P. luminescens* biosynthetic pathway either by transferring different activated sugars onto the vinyl-isocyanide aglycone **3** or by expressing redundant enzymatic functions. We constructed a series of heterologous expression vectors, which included *isnA*, *isnB*, GT1760 or GT1762, *isnA–isnB*, and *isnA–isnB*-GT1760 or -GT1762, to monitor metabolite production in *E. coli*. As expected, both *isnA* and *isnB* were required for aglycone **3** production (Fig. 2*B*). *E. coli* cells producing *isnA*, *isnB*, and either GT1760 or GT1762 redundantly produced rhabduscin and a second minor glycoside. High-resolution mass spectrometry (HR–MS) indicated that the minor compound has a molecular formula of $C_{15}H_{17}NO_5Na$ [calculated, 314.1004 $(M+Na)^+$; observed, 314.1012]. One-dimensional (^1H) NMR chemical shift and coupling constant analyses in addition to two-dimensional (gCOSY, gHSQC, gHMBC, and NOESY) correlations indicated that the minor glycoside was byelyankacin (9) (**2**) (*SI Appendix*, Table S1). The isonitrile functional group is sensitive to hydrolysis, especially in acidic conditions, and the resulting hydrolyzed formamide derivatives ($\mathbf{1}_{H_2O}$ and $\mathbf{3}_{H_2O}$) could also be detected.

The isonitrile functional group, which occurs rarely in naturally produced molecules, has a characteristic Raman resonance (observed 2,121 cm^{-1} for rhabduscin) that should be distinct for rhabduscin in *E. coli*. Robust production of rhabduscin in the heterologous host combined with its unique Raman shift enabled observation of its cellular localization by stimulated Raman scattering (SRS) microscopy (19, 20). Within the limits of spatial resolution for SRS, it was observed that rhabduscin's 2,121 cm^{-1} Raman signal was localized to the periphery of the overproducing *E. coli* cells, while the background signal in control cells lacking the gene cluster was low (Fig. 3 *A* and *B*). *E. coli* cells overproducing rhabduscin's aglycone qualitatively showed less congruency

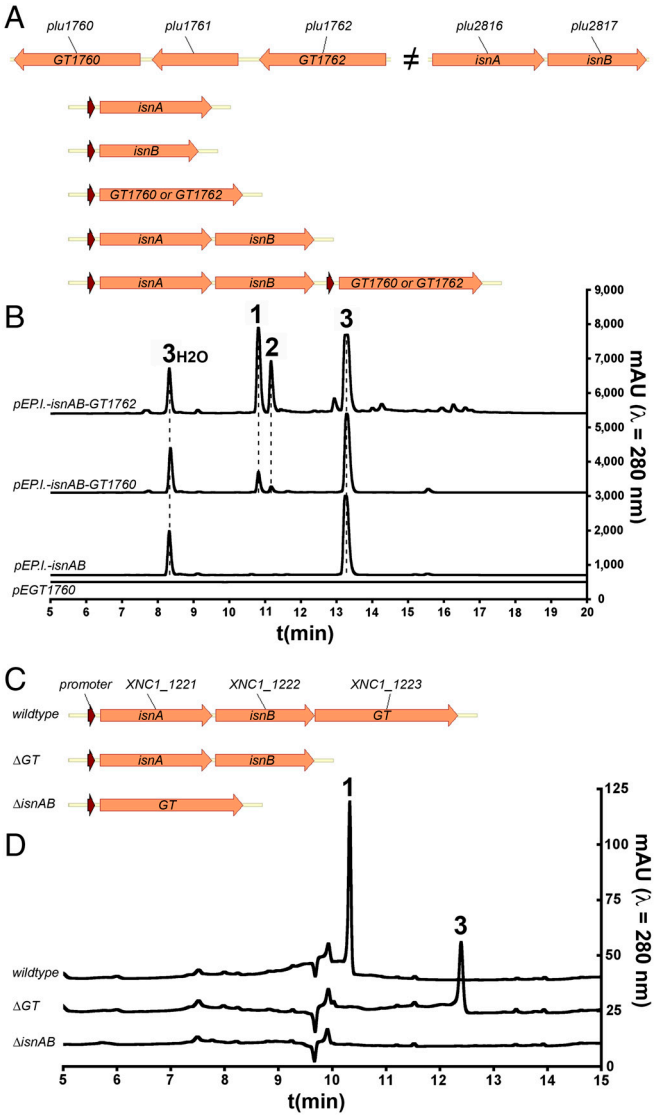

Fig. 2. (*A*) Rhabduscin biosynthetic gene cluster in *Photorhabdus luminescens* and heterologous expression of the different combinations of *P. luminescens* genes. (*B*) LC/MS ultraviolet traces and products from the heterologous expression of *P. luminescens* genes in *E. coli*. (*C*) Rhabduscin biosynthetic gene cluster in *Xenorhabdus nematophila* and genetic mutants. (*D*) LC/MS ultraviolet traces and products from *X. nematophila* wild-type, Δ*GT*, and Δ*isnAB*.

in signal localization, suggesting that the sugar substituent contributes to rhabduscin placement (*SI Appendix*, Fig. S1).

To extend these results into a wild-type host, we first constructed scarless-deletion mutants of the vinyl-isocyanide biosynthetic genes, *isnA–isnB*, and the glycosyltransferase gene in *X. nematophila* (Fig. 2*C*). *X. nematophila* was selected because we had previously found that L-proline up-regulates production of rhabduscin in this host by about an order of magnitude in rich laboratory medium (4), and also because we wanted to investigate rhabduscin's contribution to the cellular inhibition of phenoloxidase. *P. luminescens* TT01 was less suitable because it robustly produces additional phenoloxidase inhibitors belonging to the bacterial stilbene class (15), and L-proline supplementation does not stimulate rhabduscin production (4). Deletion of the *X. nematophila* glycosyltransferase alone led to accumulation of the aglycone intermediate **3**, and deletion of *isnA–isnB* completely destroyed isonitrile biosynthesis (Fig. 2*D*). Similar to the *E. coli* results described above, rhabduscin's distinct Raman signal localized to the periphery of wild-type *X. nematophila* cells,

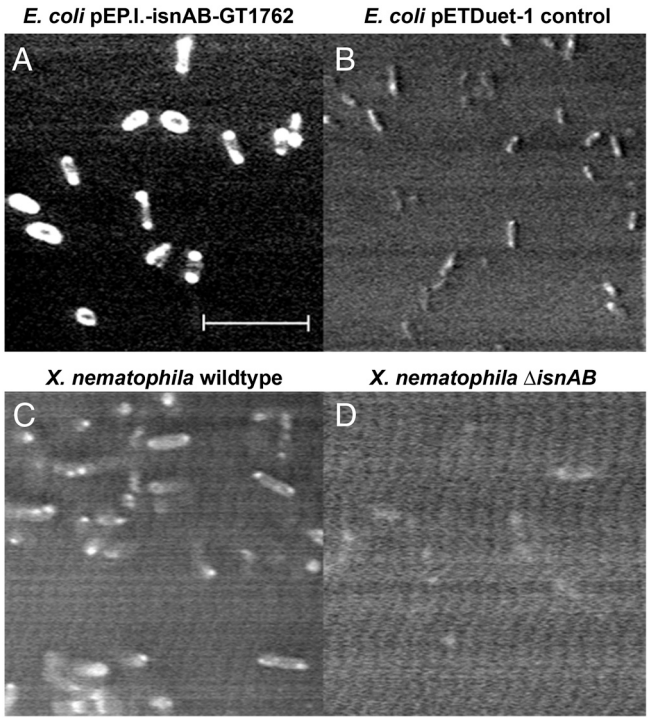

Fig. 3. SRS microscopy analyzing the spatial distribution of rhabduscin based on the vibrational resonance of the isonitrile functional group at 2,121 cm^{-1}. (Scale bar, 10 μm.) In this technique, two laser beams (pump and Stokes) with the frequency difference matching the vibrational frequency of the isonitrile group are utilized to drive the transition coherently. The spectrum is identical to spontaneous Raman spectrum but with much higher acquisition speed, allowing fast imaging (19). Because most naturally produced molecules do not have Raman signatures in this spectral region, the signal is distinctive for rhabduscin. The wild-type *X. nematophila* signal level of rhabduscin is lower than the *E. coli* overproducer, indicating lower expression level, but the difference in signal between wild-type and control cells is big enough to measure different cell phenotypes.

whereas the control Δ*isnAB* strain lacking rhabduscin only exhibited weak background signal (Fig. 3 *C* and *D*).

Synthesis of Substrate Mimics and Precursor-Directed Biosynthesis. With the heterologous glycosyltransferase expression constructs in hand, we began to investigate glycosyltransferase substrate promiscuity for the amino acid-derived part of the molecule. We challenged both *P. luminescens* glycosyltransferases individually expressed in *E. coli* with a panel of synthetic and commercial aglycone substrate mimics. We first synthesized the sterically conservative nitrile mimic **6**, which simply inverts the N—C triple bond (Fig. 4*A*). We then synthesized the azide derivative **12** (Fig. 4*B*), which could serve as a glycosyltransferase substrate mimic and allow orthogonal probes to be introduced for further cellular localization studies. The less conservative commercial mimics included *para*-coumaric acid, 4-hydroxy-benzylideneacetone, (4-hydroxybenzylidene)malononitrile, *trans*-4-hydroxy-β-nitrostyrene, and umbelliferone. Using a precursor-directed biosynthetic strategy, the synthetic nitrile **6** and the deprotected azide **12** mimics were fed to BL21(DE3) Star pLysS *E. coli* cells overexpressing GT1760 or GT1762. The products were extracted with ethyl acetate and analyzed by C_{18} reversed-phase LC/MS. The nitrile mimic was nicely converted to its corresponding rhabduscin (**7**, 46–71% conversion) or byelyankacin (**8**, 13–42%) glycoside derivatives (Fig. 4 and *SI Appendix*, Table S2), and the azide mimic was converted to its rhabduscin glycoside derivative (**13**, 61–93%). Of the commercial substrates, only benzylideneacetone and umbelliferone incorporated at minor levels (≤3%), indicating limited substrate tolerance in glycoside formation.

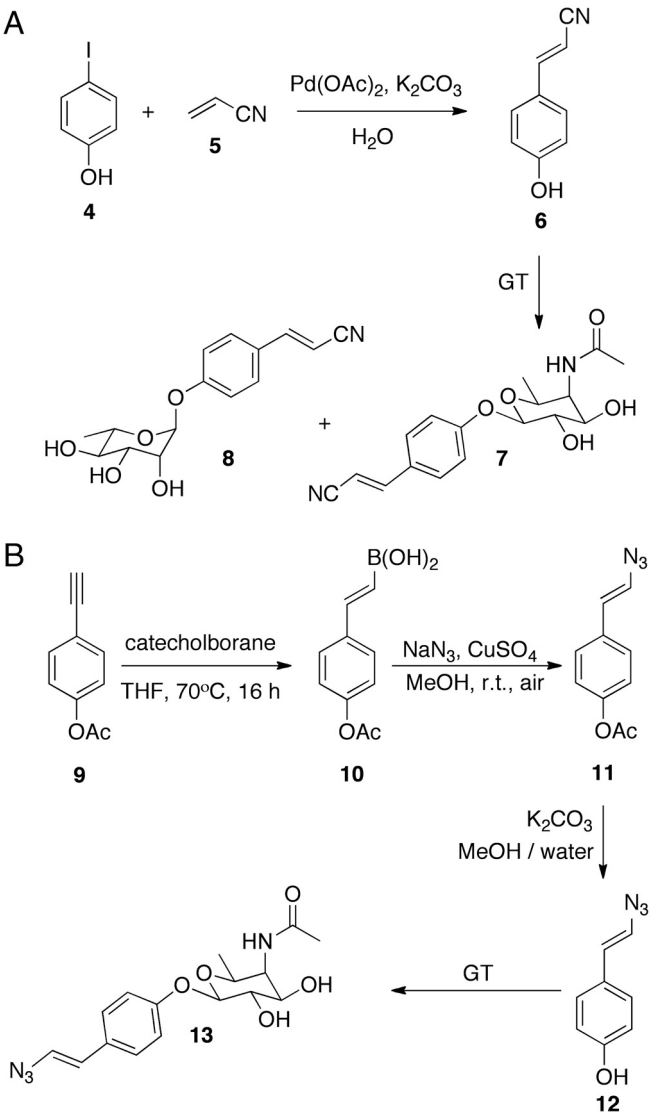

Fig. 4. Precursor-directed biosynthesis of glycoside derivatives. (*A*) (*E*)-3-(4-hydroxyphenyl)acrylonitrile (**6**) was obtained via a Heck reaction between 4-iodophenol (**4**) and acrylonitrile (**5**) (29), which resulted in a 15/85 *cis/trans* mixture. The *P. luminescens* glycosyltransferases (GTs) both glycosylated the aglycone mimic to produce glycosides **7** and **8**. (*B*) (*E*)-4-(2-azidovinyl)phenol (**12**) was obtained in three steps starting from 4-ethynylphenyl acetate (**9**); **10** was prepared by hydroboration of **9** (30); **11** was obtained via a copper-catalyzed cross-coupling between sodium azide and boronic acid **10** by adapting a previously described procedure (31); **11** was deprotected with potassium carbonate to afford phenolic compound **12**, which was accepted by the GTs to afford glycoside **13**. *SI Appendix* provides further details and spectral data.

Confocal Fluorescence Microscopic Analyses of Metabolite Localization. Because azide-aglycone mimic **12** was accepted by the glycosyltransferase in vivo to generate the azide-glycoside **13** (Fig. 4*B*), their azide chemical handles could be used to introduce bioorthogonal probes in vivo via click chemistry (21). To evaluate whether the small molecule inhibitors are accessible at the bacterial cell surface, rather than embedded in the cell membrane, we used exogenous addition of green fluorescent protein (GFP) as an easily detectable surrogate of insect phenoloxidase. In addition, to avoid competition with the natural isonitrile small molecules, we selected the *X. nematophila* strain disabled in isonitrile biosynthesis (the Δ*isnAB* strain). The glycosyltransferase was left intact in this mutant so that the synthetic mimics could be used for precursor-directed glycoside biosynthesis, bypassing

BIOCHEMISTRY

CHEMISTRY

vinyl-isonitrile biosynthesis. Stationary-phase *X. nematophila* mutant cultures supplemented with the synthetic azide **12** or the biosynthetic azide-glycoside **13** were first reacted with a biotin–alkyne conjugate, washed, and then followed by the binding of a streptavidin–GFP conjugate. Similar to the SRS results, the fluorescence localized to the periphery of the cells within the limits of resolution only in the presence of the inhibitor mimics (Fig. 5), supporting that the small molecule inhibitors would be accessible to inhibit the extracellular phenoloxidase response of an insect's innate immune system. To determine if this peripheral localization resulted from covalent linkage to the cell's peripheral lipopolysaccharide (LPS), the LPS was purified (Gentaur LPS extraction kit) and separated over a polyacrylamide gel. The fluorescent signal partitioned to an initial phenol/chloroform wash fraction, and no fluorescence was detected in the denaturing LPS gel, suggesting that localization is physical, not covalent. Further supporting a physical interaction, the isonitrile-containing molecules are present in both cell preparations and in the cleared spent medium as a diffusion product.

Metalloenzyme Inhibition: Tyrosinase and Phenoloxidase. The peripheral localization and hemolymph- or L-proline-induced up-regulation of rhabduscin suggested that it had a functional role in bacterial pathogenesis. In an earlier screen for skin-whitening agents, the α- L-rhamnopyranoside byelyankacin (**2**) was reported to be a potent tyrosinase inhibitor, the key enzyme in human melanin formation (9). Establishing whether rhabduscin plays a similar role first required establishing the absolute stereochemistry of the attached sugar, because only the relative configuration for rhabduscin was reported previously (4). Mosher ester analysis (22) indicates that rhabduscin (**1**) contains a β-L-acetamidopyranoside (*SI Appendix*, Figs. S2 and S3 and Table S3).

Given the reported activity and insect phenoloxidase's critical role in innate immune defense, we tested the compounds for inhibition against a model tyrosinase from mushroom and the phenoloxidase from waxmoth larvae (*Galleria mellonella*), a model insect host. The aglycone intermediate **3**, byelyankacin, and rhabduscin all showed low nanomolar-level inhibition (IC_{50}) against both mushroom tyrosinase and insect phenoloxidase, a level roughly three orders of magnitude more potent than the commercial whitening agent kojic acid (Table 1 and *SI Appendix*, Fig. S4). The isonitrile-containing natural products are also roughly three orders of magnitude more potent than the bacterial stilbenes from *Photorhabdus* species, which have been linked to phenoloxidase inhibition in the model tobacco hornworm larvae, *Manduca sexta* (15). Strikingly, conservative replacement of the isonitrile with the nitrile in the synthetic aglycone mimic **6** largely destroys tyrosinase inhibition, demonstrating the isonitrile's crucial role for inhibitory activity. The azide mimic **12** also exhibited weak activity. Phenoloxidases are copper-containing enzymes (23), and it is possible that the isonitrile's ability to bind copper, and other metal ions, plays a role in enzyme inhibition.

When a bacterium invades an insect host, the insect deposits melanin onto the periphery of the invading cell, which exhibits a bactericidal activity and traps the bacteria in nodules (24). To determine whether the cells themselves can inhibit tyrosinase, we subjected washed *X. nematophila* cells to tyrosinase-inhibitory assays. *X. nematophila* wild-type (initial $OD_{600} = 0.71$, 64% inhibition) and the glycosyltransferase deletion mutant (initial $OD_{600} = 0.86$, 65% inhibition) both inhibited tyrosinase activity at similar levels, whereas the isonitrile *isnAB* biosynthetic gene deletion (initial $OD_{600} = 0.77$, 0% inhibition) destroyed the cell's inhibitory activity. The inhibitory activity remained persistently associated with the cells under physiologically relevant conditions, as iterative phosphate-buffered saline (PBS) washes did not flush the activity away (*SI Appendix*, Fig. S5). Taken together, these results identify rhabduscin as a potent immunosuppressant that localizes to the periphery of the bacterial cells producing it and enables them to inhibit phenoloxidase, thereby suppressing one of the insect's primary innate immune defense strategies.

Rhabduscin is a Virulence Factor. Having obtained evidence for rhabduscin's nanomolar-level activity against phenoloxidase and its localization at or near the periphery of the bacterial cell, we wanted to determine the compound's importance in pathogenesis in an animal model. *X. nematophila* wild-type, Δ*GT*, Δ*isnAB*, and a PBS control were individually injected into the hemolymph of ten *Galleria mellonella* larvae. Wild-type bacteria killed all of the larvae within 50 h, and PBS killed none of the larvae throughout the 96 h experiment (*SI Appendix*, Fig. S6). The ΔGT mutant was less virulent than wild-type, but this bacterium grew more slowly than wild-type, presumably because of the toxicity of accumulated aglycone. The Δ*isnAB* bacteria only killed half of the larvae during the experiment, and the dead larvae were generally darker compared to the wild-type–infected dead larvae because of heigh-

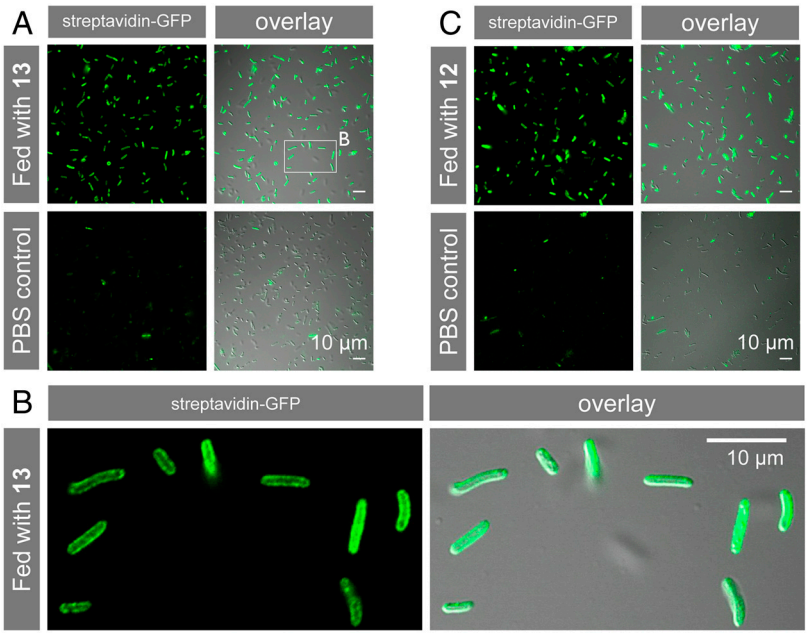

Fig. 5. Confocal fluorescence microscopy. (*A*) *X. nematophila* Δ*isnAB* fed with the two azide mimics **12** and **13** compared to PBS control. Brightness and contrast were adjusted identically for compared image sets. The azide mimics were first reacted with a biotin-alkyne conjugate followed by the binding of a streptavidin-GFP conjugate. (*B*) Enlargement of *X. nematophila* Δ*isnAB* fed with **13**. The enlarged region is indicated in *A* by the white rectangle.

Table 1. Inhibition (IC_{50}) of tyrosinase from mushroom and hemolymph-activated phenoloxidase from *Galleria mellonella* (waxmoth larvae)

Compound	Tyrosinase inhibition [nM]	Phenoloxidase inhibition [nM]
Rhabduscin (**1**)	15.1 ± 1.0	64.1 ± 2.0
Byelyankacin (**2**)	37.1 ± 2.5	184.9 ± 14.5
Aglycone-NC **3**	7.9 ± 0.8	61.7 ± 6.2
Aglycone-CN **6**	>400,000*	ND
Aglycone-N_3 **12**	>400,000*	ND
Kojic acid	22,173 ± 2,924	ND

*Low inhibitory activity precluded an accurate IC_{50} measurement.

tened melanization. These semiquantitative results demonstrate that rhabduscin contributes to an effective pathogenesis.

Isonitrile Biosynthesis in Human and Other Pathogens. The rhabduscin biosynthetic pathway is not limited to the insect pathogens *X. nematophila* and *P. luminescens*. For example, sequence analysis indicates that the related insect pathogen *Xenorhabdus bovienii* contains a homologous gene cluster (XBJ1_1355-XBJ1_1353). Like *P. luminescens*, two gene sets separated by over 1,000 genes reside in *Photorhabdus asymbiotica*, an emerging human pathogen also capable of infecting insects. *P. asymbiotica* appears to contain three adjacent copies of the glycosyltransferase (PAU_02755-PAU_02757) in addition to the *isnA* and *isnB* genes (PAU_01721-PAU_01720). The conservation across multiple *Xenorhabdus* and *Photorhabdus* species and the redundant glycosyltransferase copies in *P. luminescens* and *P. asymbiotica* emphasize the pathway's important role.

A single *isnA–isnB* fusion protein (VC1949) was reported in the related gammaproteobacterium *Vibrio cholerae* (10), the causative agent of cholera, but to date, no small molecule has been reported for this *Vibrio* pathway. We heterologously expressed a codon-optimized version of this *isnA–isnB* fusion protein in *E. coli*, but a biosynthetic small molecule product was not detected. Closer inspection of the genes surrounding VC1949 in the *V. cholerae* O1 biovar El Tor N16961 genome revealed an additional *isnB* homolog (VC1944) (*SI Appendix*, Fig. S7*A*). Coexpression of VC1949 with VC1944 or VC1944-VC1945 in *E. coli* led to aglycone **3** production (*SI Appendix*, Fig. S7*B*). Both the vinyl-isonitrile **3** and its hydrolysis product $\mathbf{3}_{H_2O}$ were observed. While it is not clear from these experiments whether **3** is further modified, based on the studies above, it is reasonable to speculate that this related pathway in *V. cholerae* contributes to pathogenesis by inhibiting metalloenzymes in the human innate immune system.

Conclusions

Gram-negative bacterial pathogens often modify their outermost LPS layer to modulate the effects of their target host's immune system (25, 26). Additionally, the LPS layer's hydrophobicity minimizes hydrophobic small molecules, including many antibiotics, from reaching the inside of the cell. Rhabduscin, byelyankacin, and their common aglycone represent another protective strategy: one in which they serve as substrate mimic inhibitors for phenoloxidase, a copper-dependent metalloenzyme that plays a central role in invertebrate immunity by depositing melanin onto the cell surface of invading microorganisms. Decorating the bacteria's outermost layer with these inhibitors provides a spatially appropriate and high local concentration to defend effectively against this terminal phenoloxidase response and thereby support the bacteria's pathogenic lifestyle.

Materials and Methods

Construction and Metabolite Analysis of Deletion Mutants. Scarless-deletion mutants of genes *isnA–isnB* and glycosyltransferase *Xn_1223* in *X. nematophila*, and subsequent product analysis of organic extracts by LC/MS, were prepared and analyzed using similar conditions as previously described (4) (*SI Appendix*, Table S4). Aliquots of stationary-phase cultures were visualized directly on poly-L-lysine-coated slides by SRS microscopy without manipulation (*SI Appendix*).

Heterologous Expression of *P. luminescens* and *V. cholerae* Genes. All genes except VC1949 were cloned into pETDuet-1 (Novagen) and expressed in BL21 (DE3) Star pLysS *E. coli* using standard molecular biological procedures (*SI Appendix*, Table S4). *E. coli* cells harboring the *P. luminescens* rhabduscin pathway or harboring the pETDuet-1 control vector were used for SRS microscopic experiments (*SI Appendix*), and aliquots of stationary-phase cells were visualized directly. A codon-optimized VC1949 in pJExpress401 was obtained from DNA2.0.

Precursor-Directed Biosynthesis of Glycoside Derivatives. BL21(DE3) Star pLysS *E. coli* containing the *P. luminescens* glycosyltransferase genes (either pEGT1760 or pEGT1762) were grown overnight at 37 °C and 250 rpm as LB suspension cultures with 0.1 mg/mL ampicillin. Fifty-μL aliquots of overnight stationary-phase culture were used to inoculate 5-mL portions of M9 minimal medium supplemented with 0.5% (m/vol) casamino acids and 0.1 mg/mL ampicillin. The cultures were grown at 37 °C and 250 rpm to an OD_{600} = 0.5–0.6. Glycosyltransferase gene expression was induced with IPTG (1 mM final) and supplemented with small molecule precursors (100 μM) in DMSO. The induced cultures were incubated at 25 °C and 250 rpm to a final time of 24 h. The whole cultures were rigorously extracted with 5 mL of ethyl acetate, separated by centrifugation; the top 4 mL of ethyl acetate was transferred to a glass vial and dried, and the resulting residue was dissolved in 500 μL methanol for reversed-phase LC/MS analysis.

Chemoenzymatic Synthesis of Rhabduscin-Azide (13). Two 4-L Erlenmeyer flasks, each containing 1 L of M9 minimal medium supplemented with casamino acids (0.5%) and ampicillin (0.1 g/L), were inoculated with 5 mL of an overnight BL21(DE3) Star pLysS *E. coli* culture harboring pEGT1762 (LB, 0.1 mg/mL of ampicillin). The cultures were grown at 37 °C and 250 rpm to an OD_{600} = 0.5–0.6. Expression of the cluster was induced by the addition of IPTG (1 mM final), and, at the same time, synthetic (**12**) (32 mg, 0.20 mmol) dissolved in DMSO (5 mL) was added to each culture. The cultures were grown at 25 °C and 250 rpm for a total time of 24 h. The combined whole cultures were extracted with ethyl acetate (three times, 2 L total). The combined organic fractions were dried (Na_2SO_4), filtered, and concentrated under reduced pressure to afford an orange solid (220 mg). The residue was purified by preparative HPLC (Luna C_{18}, 5 μm, 250 • 21.2 mm, Phenomenex) with an acetonitrile : water gradient at 10 mL/ min: 0–15 min, 30% to 45% acetonitrile; 15–16 min, 45% to 100% acetonitrile; and 16–21 min, 100% acetonitrile. The combined fractions (retention time = 13 min) were concentrated under reduced pressure to afford (**13**) as a pale yellow compound (9.0 mg, 0.026 mmol, 6.5%). ^{1}H-NMR: (600 MHz, CD_3OD) δ 7.28 (d, J = 8.8 Hz, 2H), 7.00 (d, J = 8.8 Hz, 2H), 6.78 (d, J = 13.8 Hz, 1H), 6.21 (d, J = 13.8 Hz, 1H), 4.85 (m, 1H), 4.29 (dd, J = 4.7, 1.4 Hz, 1H), 3.92 (qd, J = 1.4, 6.4 Hz, 1H), 3.78 (dd, J = 10.0, 4.7 Hz, 1H), 3.67 (dd, J = 10.0, 7.6 Hz, 1H), 2.05 (s, 3H), 1.17 (d, J = 6.4 Hz, 3H). ^{13}C NMR: (151 MHz, CD_3OD) δ 174.8, 158.4, 131.0, 128.0, 126.9, 120.1, 117.9, 102.7, 73.6, 72.3, 71.2, 54.9, 22.5, 17.0. HR-MS: (ESI) calculated for $C_{16}H_{20}N_4O_5Na$ 371.1331 $(M + Na)^+$, found 371.1335.

Mushroom Tyrosinase-Inhibition Assay. Mushroom tyrosinase was purchased from Sigma–Aldrich (T3824). The assay was adapted from the Pomerantz method (27), using 96-well plates (costar 3370) with the absorbance being monitored in a Molecular Devices FlexStation 3. Fifty μL of a 2-mM DOPA solution in 0.1-M phosphate buffer (pH 6.8) was added to 50 μL of the inhibitor (varying concentrations) dissolved in 10% DMSO in water. The resulting solution was incubated for 10 min at room temperature before the addition of 50 μL of a 135-U/mL mushroom tyrosinase solution in phosphate buffer. The 96-well plate was agitated for 3 s before starting to measure absorbance at 475 nm every 20 s. Kojic acid was used as a positive control and a 10% DMSO water solution was used as a blank. The initial rate was obtained by linear regression of the first 3 min of dopachrome formation. The fractional activity was obtained by dividing the inhibited rate by the uninhibited rate obtained from the blank reaction. The inhibition curves and IC_{50} values were calculated using nonlinear regression sigmoid GraphPad with Prism 5 for Windows.

Mushroom Tyrosinase Inhibition Using *X. nematophila* Cells. The cell-inhibition assay was conducted similarly to the small molecule-inhibition assay described above, but a suspension of cells was used as the inhibitor. *X. nematophila* wild-type, Δ*isnAB*, and ΔGT mutants were grown overnight in

suspension (5 mL of LB) from a single colony at 30 °C and 250 rpm. Five-mL cultures (2-g tryptone, 5-g yeast extract, and 10-g NaCl per L supplemented with 0.1 M final of L-proline) were inoculated with 100 μL of the overnight culture and grown at 30 °C and 250 rpm for 48 h. The cells were centrifuged and washed once with PBS before being diluted to an OD_{600} of approximately 0.75 for use in the assay described above. To assess inhibitor persistence on the cells, a subsequent experiment was conducted with iterative washing steps. Here, *X. nematophila* was grown and analyzed exactly the same, except cellular inhibition was measured after each successive wash cycle. A 15-mL bacterial suspension was washed 14 times with PBS by centrifugation (800 × *g*, 5 min) and cell resuspension. At each washing round, an aliquot of 500 μL of cell suspension was removed for analysis, and the volume of PBS added for the next washing round was reduced by 500 μL to minimize cell dilution.

Hemolymph Phenoloxidase–Inhibition Assay. The assay was a modification of the procedure described by Eleftherianos et al. (28). Waxmoth larvae were chilled on ice for 15 min before sterilizing their surface with 70% ethanol. The larvae were then decapitated and bled into a Falcon tube on ice. The collected hemolymph was diluted in a 3:1 (vol/vol) ratio with PBS (50 mM, pH = 6.5) and centrifuged at 14,700 × *g* and 4 °C for 10 min to obtain the plasma. Activation of the phenoloxidase was performed directly in the 96-well assay plate. Ten μL of diluted hemolymph plasma were added to 2 μL of *E. coli* LPS (5 mg/mL; Sigma-Aldrich) for activation and 115 μL of PBS (50 mM, pH = 6.5), and the solution was kept at room temperature for 1 h. Then, 50 μL of the inhibitor dissolved in 10% DMSO in PBS followed by 25 μL of 20-mM 4-methyl catechol were added. The 96-well plate was agitated for 3 s before starting to measure absorbance at 490 nm every min for 1 h. IC_{50} values were obtained as described for the tyrosinase-inhibitory assays.

Preparation of Cells for Confocal Fluorescence Microscopy. *X. nematophila* Δ*isnAB* was grown overnight in suspension (5 mL of LB) from a single colony at 30 °C and 250 rpm. Five-mL cultures (2-g tryptone, 5-g yeast extract, and 10-g NaCl per L, and 0.1 M of L-proline) were inoculated with 150 μL of the overnight culture and were grown at 30 °C and 250 rpm for 6 h before adding 25 μL of DMSO stock solution of **12**, **13**, or blank (100 μM final). The cultures were grown for 72 h at 30 °C and 250 rpm, where 25 μL of DMSO or azide **12** or **13** stock solutions were added after 29 and 56 h. Aliquots of 500 μL were centrifuged at 4,500 × *g* for 5 min and the cells were then washed with 500 μL PBS and centrifuged. The cells were then reacted with PEG4 carboxamide-propargyl biotin (3 μM final, Invitrogen B10185) using Click-iT Cell Buffer Kit (Invitrogen C10269) following the supplier's procedure. The only modification to the supplier's procedure was that the cells were resuspended in half the volume of buffer before adding the second half of the buffer mixed with the active compounds. After 30 min of reaction time, the cells were centrifuged at 1,500 × *g* for 4 min and washed three times with 500 μL of PBS before being resuspended in 500 μL PBS. A solution of 100 μL PBS and 10 μL streptavidin-*Renilla reniformis* GFP (Avidity, 320 mg/mL) was added to a 100-μL aliquot, and the mixture was reacted for 15 min at room temperature. The cells were then centrifuged at 1,500 × *g* for 4 min and washed two times with PBS before being resuspended in 100 μL PBS for microscopy.

Waxmoth Larvae Survival After *X. nematophila* Infection. Waxmoth larvae (*Galleria mellonella*) were obtained from Berkshire Biological. Virulence assays were adapted from Eleftherianos et al. (28). *X. nematophila* wild-type, Δ*isnAB*, and ΔGT were grown overnight in liquid culture (5 mL, LB) at 30 °C and 250 rpm. One hundred μL of the overnight cultures were centrifuged (6 min at 3,300 × *g*), the spent medium was discarded, and the cells were resuspended in 1 mL of PBS. The quantity of cells was estimated with OD_{600} (estimation: 10^9 cells/mL for $OD_{600} = 1$). The suspension was diluted to obtain an approximate concentration of 100, 1,000, and 10,000 cells per 10 μL. Prior to injection, the rear ends of the larvae were washed with 70% ethanol. The larvae were then injected into the hemocoel with 10 μL of cell suspension using 31-gauge disposable insulin syringes (BD). PBS-injected insects served as a control set. Larvae were kept at room temperature with food, and mortality (no reaction when poked) was monitored for 100 h. Ten larvae were used for each condition.

ACKNOWLEDGMENTS. We thank Xiaoliang Sunney Xie (Harvard University, Cambridge, MA) for facilitating SRS microscopic measurements in his lab. We thank Shugeng Cao (Harvard Medical School, Boston, MA) for helpful discussions and reviewing a preliminary version of the manuscript. We also thank Jennifer C. Waters and Wendy C. Salmon at the Harvard Medical School Nikon Imaging Center (Boston, MA) for assistance with confocal fluorescence microscopy. This work was supported by National Institutes of Health Grant R01 GM086258 (to J.C.); National Institutes of Health Pathway to Independence Award (Grant 1K99 GM097096-01, to J.M.C.); a Damon Runyon Cancer Research Foundation postdoctoral fellowship (DRG-2002-09, to J.M.C.); and the Swiss National Science Foundation (PBELP2-130880, to C.P.).

1. Herbert EE, Goodrich-Blair H (2007) Friend and foe: The two faces of *Xenorhabdus nematophila*. *Nat Rev Microbiol* 5:634–646.
2. Richards GR, Goodrich-Blair H (2009) Masters of conquest and pillage: *Xenorhabdus nematophila* global regulators control transitions from virulence to nutrient acquisition. *Cell Microbiol* 11:1025–1033.
3. Waterfield NR, Ciche T, Clarke D (2009) *Photorhabdus* and a host of hosts. *Annu Rev Microbiol* 63:557–574.
4. Crawford JM, Kontnik R, Clardy J (2010) Regulating alternative lifestyles in entomopathogenic bacteria. *Curr Biol* 20:69–74.
5. Chaston JM, et al. (2011) The entomopathogenic bacterial endosymbionts *Xenorhabdus* and *Photorhabdus*: Convergent lifestyles from divergent genomes. *PLoS One* 6:e27909.
6. Brady SF, Clardy J (2005) Cloning and heterologous expression of isocyanide biosynthetic genes from environmental DNA. *Angew Chem Int Ed Engl* 44:7063–7065.
7. Brady SF, Clardy J (2005) Systematic investigation of the *Escherichia coli* metabolome for the biosynthetic origin of an isocyanide carbon atom. *Angew Chem Int Ed Engl* 44:7045–7048.
8. Duchaud E, et al. (2003) The genome sequence of the entomopathogenic bacterium *Photorhabdus luminescens*. *Nat Biotechnol* 21:1307–1313.
9. Takahashi S, et al. (2007) Byelyankacin: A novel melanogenesis inhibitor produced by *Enterobacter* sp. B20. *J Antibiot (Tokyo)* 60:717–720.
10. Brady SF, Bauer JD, Clarke-Pearson MF, Daniels R (2007) Natural products from *isnA*-containing biosynthetic gene clusters recovered from the genomes of cultured and uncultured bacteria. *J Am Chem Soc* 129:12102–12103.
11. Uvell H, Engstrom Y (2007) A multilayered defense against infection: Combinatorial control of insect immune genes. *Trends Genet* 23:342–349.
12. Cerenius L, Kawabata S, Lee BL, Nonaka M, Soderhall K (2010) Proteolytic cascades and their involvement in invertebrate immunity. *Trends Biochem Sci* 35:575–583.
13. Cerenius L, Lee BL, Soderhall K (2008) The proPO-system: Pros and cons for its role in invertebrate immunity. *Trends Immunol* 29:263–271.
14. Eleftherianos I, Revenis C (2011) Role and importance of phenoloxidase in insect hemostasis. *J Innate Immun* 3:28–33.
15. Eleftherianos I, et al. (2007) An antibiotic produced by an insect-pathogenic bacterium suppresses host defenses through phenoloxidase inhibition. *Proc Natl Acad Sci USA* 104:2419–2424.
16. Waterfield NR, et al. (2008) Rapid virulence annotation (RVA): Identification of virulence factors using a bacterial genome library and multiple invertebrate hosts. *Proc Natl Acad Sci USA* 105:15967–15972.
17. Eleftherianos I, ffrench-Constant RH, Clarke DJ, Dowling AJ, Reynolds SE (2010) Dissecting the immune response to the entomopathogen *Photorhabdus*. *Trends Microbiol* 18:552–560.
18. Vallenet D, et al. (2009) MicroScope: A platform for microbial genome annotation and comparative genomics. *Database (Oxford)* 2009:bap021.
19. Freudiger CW, et al. (2008) Label-free biomedical imaging with high sensitivity by stimulated Raman scattering microscopy. *Science* 322:1857–1861.
20. Saar BG, et al. (2010) Video-rate molecular imaging in vivo with stimulated Raman scattering. *Science* 330:1368–1370.
21. Prescher JA, Bertozzi CR (2005) Chemistry in living systems. *Nat Chem Biol* 1:13–21.
22. Hoye TR, Jeffrey CS, Shao F (2007) Mosher ester analysis for the determination of absolute configuration of stereogenic (chiral) carbinol carbons. *Nat Protoc* 2:2451–2458.
23. Li Y, Wang Y, Jiang H, Deng J (2009) Crystal structure of *Manduca sexta* prophenoloxidase provides insights into the mechanism of type 3 copper enzymes. *Proc Natl Acad Sci USA* 106:17002–17006.
24. Feldhaar H, Gross R (2008) Immune reactions of insects on bacterial pathogens and mutualists. *Microbes Infect* 10:1082–1088.
25. Raetz CR, Whitfield C (2002) Lipopolysaccharide endotoxins. *Annu Rev Biochem* 71:635–700.
26. Raetz CR, Reynolds CM, Trent MS, Bishop RE (2007) Lipid A modification systems in gram-negative bacteria. *Annu Rev Biochem* 76:295–329.
27. Pomerantz SH (1963) Separation, purification, and properties of two tyrosinases from hamster melanoma. *J Biol Chem* 238:2351–2357.
28. Eleftherianos I, Millichap PJ, ffrench-Constant RH, Reynolds SE (2006) RNAi suppression of recognition protein mediated immune responses in the tobacco hornworm *Manduca sexta* causes increased susceptibility to the insect pathogen *Photorhabdus*. *Dev Comp Immunol* 30:1099–1107.
29. Bumagin NA, More PG, Beletskaya IP (1989) Synthesis of substituted cinnamic acids and cinnamonitriles via palladium catalyzed coupling reactions of aryl halides with acrylic acid and acrylonitrile in aqueous media. *J Organomet Chem* 371:397–401.
30. Churches QI, et al. (2008) Stereoselectivity of the Petasis reaction with various chiral amines and styrenylboronic acids. *Pure Appl Chem* 80:687–694.
31. Tao C-Z, et al. (2007) Copper-catalyzed synthesis of aryl azides and 1-aryl-1,2,3-triazoles from boronic acids. *Tetrahedron Lett* 48:3525–3529.